

STRESS INTENSITY FACTOR DISTRIBUTION AND CRACK GROWTH IN PRESSURE VESSEL PROBLEMS BY THE FROZEN STRESS METHOD

C. W. Smith¹ and C. T. Liu²

¹ Department of Engineering Science and Mechanics
Virginia Polytechnic Institute and State University
Blacksburg, Virginia 24061

² Air Force Research Laboratory, PRSM
10 E. Saturn Blvd.
Edwards AFB, California 93524-7680

ABSTRACT

This paper describes the application of a laboratory based experimental method [1] to three dimensional cracked body problems in pressure vessels in order to determine the crack shape and stress intensity factor (SIF) distribution along the crack front when the crack shape is not known a-priori. Results for specific problems are presented and conditions and limitation of the method are described.

INTRODUCTION

Back in the mid sixties, when an explosion of three dimensional fracture problems solutions developed along with the digital computer, the writer and his associates decided that a laboratory based experimental method should be developed in order to partially fill the gap produced by the lack of proof testing for many large structures, such as ships, bridges,

aircraft, missiles and pressure vessels because of the excessive costs involved. By effecting a marriage between the equations of linear elastic fracture mechanics (LEFM) with frozen stress photoelasticity (Appendix A), such a method has been developed. Over the years, it has been used to check many numerical solutions in a cost effective manner and, in the process has provided some novel, or unique aspects. The method of analysis with equations for all three local modes of stress intensity is described in [1], and is also presented in [2]. The unique feature lies in the fact that fact that starter cracks may be grown above critical temperature by applying service loads before cooling the model. When the crack reaches its desired size and shape (controlled only by loads and body shape) the loads are reduced in order to stop crack growth and stress freezing is then completed. If sufficient growth is permitted to occur, only Mode I will exist along the crack front. That is, as described by Cotterell [3], [4] the crack is a Class I crack, and

Approved for public release; distribution unlimited.

Report Documentation Page

*Form Approved
OMB No. 0704-0188*

Public reporting burden for the collection of information is estimated to average 1 hour per response, including the time for reviewing instructions, searching existing data sources, gathering and maintaining the data needed, and completing and reviewing the collection of information. Send comments regarding this burden estimate or any other aspect of this collection of information, including suggestions for reducing this burden, to Washington Headquarters Services, Directorate for Information Operations and Reports, 1215 Jefferson Davis Highway, Suite 1204, Arlington VA 22202-4302. Respondents should be aware that notwithstanding any other provision of law, no person shall be subject to a penalty for failing to comply with a collection of information if it does not display a currently valid OMB control number.

1. REPORT DATE 14 JUN 2004	2. REPORT TYPE	3. DATES COVERED -	
4. TITLE AND SUBTITLE Stress Intensity Factor Distribution and Crack Growth in Pressure Vessel Problems by the Frozen Stress Method		5a. CONTRACT NUMBER	
		5b. GRANT NUMBER	
		5c. PROGRAM ELEMENT NUMBER	
6. AUTHOR(S) C Smith; C Liu		5d. PROJECT NUMBER 2302	
		5e. TASK NUMBER 0378	
		5f. WORK UNIT NUMBER 23020378	
7. PERFORMING ORGANIZATION NAME(S) AND ADDRESS(ES) Air Force Research Laboratory (AFMC), AFRL/PRS, 5 Pollux Drive, Edwards AFB, CA, 93524-7048		8. PERFORMING ORGANIZATION REPORT NUMBER	
9. SPONSORING/MONITORING AGENCY NAME(S) AND ADDRESS(ES)		10. SPONSOR/MONITOR'S ACRONYM(S)	
		11. SPONSOR/MONITOR'S REPORT NUMBER(S)	
12. DISTRIBUTION/AVAILABILITY STATEMENT Approved for public release; distribution unlimited			
13. SUPPLEMENTARY NOTES			
14. ABSTRACT This paper describes the application of a laboratory based experimental method [1] to three dimensional cracked body problems in pressure vessels in order to determine the crack shape and stress intensity factor (SIF) distribution along the crack front when the crack shape is not known a-priori. Results for specific problems are presented and conditions and limitation of the method are described.			
15. SUBJECT TERMS			
16. SECURITY CLASSIFICATION OF:			17. LIMITATION OF ABSTRACT
a. REPORT unclassified	b. ABSTRACT unclassified	c. THIS PAGE unclassified	
			18. NUMBER OF PAGES 8
			19a. NAME OF RESPONSIBLE PERSON

by using data sufficiently close to the crack tip, a two term expression for the local stresses becomes adequate for analysis. The resulting equations for both mixed and pure Mode I are presented in Appendix B.

EXPERIMENTAL RESULTS

Nozzle Corner Cracks in Reactor Vessels

The writer and his associates were approached by researchers at Delft Technical University in 1976 to evaluate a test developed at Delft for determining stress intensity factors for a nozzle corner crack. They used a flat plate with a nozzle located in its center with a starter crack oriented normal to an external field of uniaxial tension [5]. They grew the crack in a steel model using high cycle tension-tension fatigue loads. The result is shown in Fig 1a for small and moderately deep cracks and in Fig 1c for a deep crack. Using monotonic loads, we produced shapes shown in Figs 1b and 1d which overlaid those obtained at Delft.

We subsequently applied our method to study a similar local geometric situation where the nozzle was located in a scale model of a nuclear pressure vessel. (Fig. 2). The model consisted of two semi-cylindrical center sections, each containing a nozzle and two hemispherical end domes. Starter cracks were oriented as shown in Fig. 3a and the model was loaded by internal pressure. The crack shapes and normalized SIF distributions obtained are shown in Fig. 3b and Fig. 3c respectively. Also shown in Fig. 3b are the loci of fitted ellipses used by analysts in this problem. Fig. 3c shows how the flattening of the crack shapes near their mid points effectively inverts the SIF distribution along the crack front. When a starter crack was inserted into several models at the $\theta = 45^\circ$ location, (Fig. 3a) very different results occurred. First, the planar starter crack (shaded in Fig. 4a) grew in its plane near n to n' . However, it followed a gently curved path from m to v . The normalized SIF distributions initially showed a domed distribution with peak values near $\beta/\beta_{max} \approx 0.5$ (Fig. 4b). However, between $a'/T' = 0.291$ and 0.458 , a

crease in the crack surface between the planar and curved parts of the crack surface smoothed out and the SIF distribution inverted with the maximum SIF values occurring at $\beta/\beta_{max} \approx 1.0$ (Fig. 4b). It is noted here that the near tip fringe patterns along the curved portion of the crack were not symmetrical with respect to the crack surface, but no rotation of the fringe loops was present to indicate a shear mode, the lack of symmetry in the fringe loops was due to a varying non-singular tensile stress parallel to the crack growth direction and was not indicative of a shear mode [6]. Generally, the shape taken by the growing crack is the one which minimizes the gradient in the SIF along the flaw border.

Cracks in Rocket Grain

In all of the cases discussed above the starter cracks were, in fact, Class I Cracks. Since, however, they are introduced by striking a sharp blade held normal to a surface, and the resulting crack emanates from the blade tip, the loading for the starter crack is a dynamic wedging force and the induced stress field may differ from internal pressure. This might occur if one drives the starter crack too far in. If the load is then changed to internal pressure, the new load may produce a shear mode at the starter crack tip. In such cases, the crack will then turn in order to eliminate the shear mode as it grows. An example of this type of behavior follows. Figure 5 shows a 1/10 scale model of the crosssection of a cylindrical motor grain model. Two off axis (Fig. 5) cracks were introduced in different models but in identical loci of each of the models. Plan and center section *SS* views of the cracks are shown in Fig. 6. The crack in Model 4 has not grown as far as the one in Model 8. If one assumes that the crack in Model 8 represents a later stage in the growth of the crack in Model 4, one can construct the following scenario. Table I gives pertinent data from the frozen stress tests on the two cracks. The normalized (SIFs) F_1 were computed using an approximation of an elliptical integral of the second kind \sqrt{Q} , which

Approved for public release; distribution unlimited.

amounts to assuming that the cracks were planar semi-elliptic shapes. While this assumption does in fact hold for symmetric cracks (Fig. 5) which enjoy both geometric and load symmetry, such is not the case of the “off axis” cracks pictured in Fig. 6, as noted by the direction change in the crack fronts shown in the section *SS* cuts. The influence of these direction changes, while accommodated in the experimental data, was ignored in computing the values of \sqrt{Q} for use in determining F_i . The form of \sqrt{Q} was developed by Newman [7]. We note that, in our scenario, Model 4 represents an earlier state in the growth of the off-axis crack and that Model 8 indicates a larger crack. Model 4 exhibited both F_1 and F_2 values all along the crack front except at the fin boundary where only F_1 existed, and section *SS* shows the crack front turning. In Model 8, however, we see a series of river marks on both sides of the crack suggesting the presence of Mode III. No data were taken in these regions however, since it was conjectured that the limitations of linear elastic fracture mechanics may have been exceeded. At all other locations along the Model 8 crack front, however, only pure Mode I was measured suggesting that the crack had grown sufficiently to eliminate all shear modes. The section *SS* in Model 8 suggests that the turn in Model 4 (which was accompanied by Mode II) has been completed. This means that the crack in Model 8 has achieved, or nearly achieved, Class I status with turning completed and will now proceed in the new direction indicated by Section *SS* (Fig. 6). It should also be noted that in Model 8, a slight dimple appears in the crack front in the areas of the river markings, suggesting that the effect of shear modes is to retard temporarily the growth of the crack.

Such a scenario as described above leads to an interesting conclusion. Both frozen stress experiments and finite element analysis point to the fin corner as the highest stressed point in the uncracked loaded model. However, any crack initiating there will contain shear modes. On the other hand, a crack initiating on the fin axis (i.e. the symmetric crack in Fig. 5) will show no evidence of shear modes (Fig.

7) and is a Class 1 crack when it appears. As such, one expects such a crack to be far more mobile and dangerous than one emanating from the fin corner. Thus, one cannot predict a fracture on the basis of uncracked model stress analysis alone. According to Cotterell, all Class II cracks (ie here those under shear modes) eventually become Class I cracks and this concept is borne out by these results. The symmetric crack shown in Fig. 5 is already a Class I crack due to absence of shear modes and will not turn during growth.

On the basis of the examples presented above (and other cases studied), we conclude that stable crack growth in pressure vessels proceeds under pure Mode I. Moreover, cracks grown above critical temperature during the stress freezing process in photoelastic models appear to overlay those produced in steel structures by high cycle tension-tension fatigue when test scales are identical.

Table 1

Loads ¹	Crack Description ² (dimensions in mm)	³ $F_i = K_i \sqrt{Q} / P_i \sqrt{\pi \alpha}$ $i = 1, 2$			Fin tip surface
		Depth (d)	Surface (s)		
P = 88.97 N P _{max} = 0.049 MPa P _{sf} = 0.035 MPa	Model 4 Off-axis inclined $\alpha = 8.71$ $\Delta\alpha = 2.18$ $c = 11.15$ $\Delta c = 3.02$ $a/c = 0.78$ $\alpha/t = 0.23$	$F_1 = 2.09$ $F_2 = 0.53$	ns 20° 2.88	ns 20° 2.81	
	Model 8 Off-axis inclined $\alpha = 12.50$ $\Delta\alpha = 3.4$ $c = 21.1$ $\Delta c = 10.4$ $a/c = 0.59$ $\alpha/t = 0.34$		2.19	ns 30° 2.33	
		* F_1 values			

Notations:

1. P = axial compressive load
P_{max} = maximum internal pressure to grow crack
P_{sf} = stress freezing pressure
2. α = crack depth; $\Delta\alpha$ = crack length growth
c = half length of crack in fin tip surface; Δc = half crack growth in fin tip surface
3. \sqrt{Q} = approximation of elliptic integral of second kind

$$Q = 1 + 1.464 \left(\frac{\alpha}{c} \right)^{1.65} \quad \frac{\alpha}{c} \leq 1 \quad Q = 1.464 \left(\frac{\alpha}{c} \right)^{1.65} \quad \frac{\alpha}{c} > 1$$

All flaws were characterized as semi-elliptic flaws of depth α and length $2c$.

However, off-axis cracks were neither perfectly semi-elliptic nor planar.

4. ns = near surface slices were used in place of surface slices to avoid a possible surface fringe
5. Slices at $\theta = 60^\circ$ revealed a shear mode in Model 4 but not in Model 8.

Approved for public release; distribution unlimited.

ACKNOWLEDGEMENT

The writers wish to acknowledge the support of Oak Ridge National Laboratory Under Contract No. W7405-Eng-26 and P.O. No. RPO 10230 with ERC Inc. through AFRL at Edwards Air Force Base.

REFERENCES

- [1] Smith, C. W., "Experimental Determination of Stress Intensity Factor Distributions in Engineering Problems," *Applied Mechanics Reviews*, Vol. 46, No. 11, Part 2, pp. 529-540, November 1993.
- [2] Smith, C. W. and Kobayashi, A. S., Chapter 20 of *Handbook on Experimental Mechanics*, A. S. Kobayashi, Ed., pp. 891-956 Prentice-Hall, 1987.
- [3] Cotterell, B., "On Brittle Fracture Paths," *International Journal of Fracture Mechanics*, Vol. 1, pp. 96-103, 1965.
- [4] Cotterell, B. "Notes on Paths and Stability of Cracks," *International Journal of Fracture Mechanics*, Vol. 2, pp. 526-533, 1966.
- [5] Broekhoven, M. J. G., "Computation of Stress Intensity Factors for Nozzle Corner Cracks by Various Finite Element Procedures," Report MMPP 119, Delft University of Technology, Laboratory for Thermal Power and Nuclear Engr. Paper G 416 3rd SMIRT Conference London 1975.
- [6] Smith, C. W. and Wiersma, S. J., "Stress Fringe Signatures for Propagating Cracks," *Journal of Engineering Fracture Mechanics*, Vol. 23, No. 1, pp. 229-236, 1986.
- [7] Newman, J. C., Jr., Fracture Analysis of Surface and Through Cracks in Cylindrical Pressure Vessels, NASA-TN-D8325, Dec. 1976.

APPENDIX A- Frozen Stress Photoelasticity

When a transparent model is placed in a circularly polarized monochromatic light field and loaded, dark fringes will appear which are proportional to the

Approved for public release; distribution unlimited.

applied load. These fringes are called stress fringes or isochromatics, and the magnitude of the maximum in-plane shear stress is a constant along a given fringe.

Some transparent materials exhibit mechanical diphasic characteristics above a certain temperature, called the critical temperature (T_c). The material, while still perfectly elastic will exhibit a fringe sensitivity of about twenty times the value obtained at room temperature, and its modulus of elasticity will be reduced to about one six-hundredth of its room temperature value. By raising the model temperature above T_c , loading, and then cooling slowly to room temperature, the stress fringes associated with T_c will be retained when the material is returned to room temperature. Since the material is so much more sensitive to fringe generation above T_c than at room temperature, fringe recovery at room temperature upon unloading is negligible. The model may then be sliced without disturbing the "frozen in" fringe pattern and analyzed as a two-dimensional model but containing the three-dimensional effects. In the use of the method to make measurements near crack tips, due to the need to reduce loads above critical temperature to preclude large local deformations, and the use of thin slices, few stress fringes are available by standard procedures. To overcome this obstacle, a refined polariscope is employed to allow the tandem use of the Post and Tardy methods to increase the number of fringes available locally.

In fringe photographs, integral fringes are dark in a dark field and bright in a bright field.

Appendix B

Mode I Algorithm

Beginning with the Griffith-Irwin Equations, we may write, for Mode I, for the homogeneous case,

$$\sigma_{ij} = \frac{K_1}{(2\pi r)^{\frac{1}{2}}} f_{ij}(\theta) + \sigma_{ij}^{\circ} \quad (i, j = n, z) \quad (1)$$

where:

σ_{ij} are components of stress

K_1 is SIF

r, θ are measured from crack tip (Fig. B-1)

σ_{ij}° are non-singular stress components

Then, along $\theta = \pi/2$, after truncating σ_{ij}

$$\tau_{nz}^{max} = \frac{K_1}{(8\pi r)^{\frac{1}{2}}} + \tau^\circ = \frac{K_{AP}}{(8\pi r)^{\frac{1}{2}}} \quad (2)$$

where:

$\tau^\circ = f(\sigma_{ij}^\circ)$ and is constant over the data range

K_{AP} = apparent SIF

τ_{nz}^{max} = maximum shear stress in nz plane

Normalizing with respect to $\bar{\sigma}$,

$$\therefore \frac{K_{AP}}{\bar{\sigma}(\pi a)^{\frac{1}{2}}} = \frac{K_1}{\bar{\sigma}(\pi a)^{\frac{1}{2}}} + \frac{\sqrt{8}\tau^\circ}{\bar{\sigma}} \left(\frac{r}{a}\right)^{\frac{1}{2}} \quad (3)$$

where (Fig. B-1) a = crack length, and $\bar{\sigma}$ = remote normal stress

i.e. $\frac{K_{AP}}{\bar{\sigma}(\pi a)^{\frac{1}{2}}}$ vs. $\sqrt{\frac{r}{a}}$ is linear.

From the Stress-Optic Law, $\tau_{nz}^{max} = nf/2t$ where,

n = stress fringe order,

f = material fringe value, and

t = specimen (or slice) thickness

then from Eq. 2

$$K_{AP} = \tau_{nz}^{max} (8\pi r)^{\frac{1}{2}} = \frac{nf}{2t} (8\pi r)^{\frac{1}{2}}$$

where K_{AP} (through a measure of n) and r become the measured quantities from the stress fringe pattern at different points in the pattern.

In part of the present study, instead of normalizing K with respect to $\bar{\sigma}(\pi a)^{1/2}$, we have selected $p_{sf}\sqrt{\pi a}/Q$ as the normalizing factor where \sqrt{Q} is an elliptic integral of the second kind approximated here, as shown in Table I. An example of the determination of F_1 in Table I from test data is given in Fig. B-2.

Mixed Mode Algorithm

The mixed mode algorithm was developed (see Fig. B-3) by requiring that:

Approved for public release; distribution unlimited.

$$\lim_{\substack{r_m \rightarrow 0 \\ \theta_m \rightarrow \theta_m^\circ}} \left\{ (8\pi r_m)^{1/2} \frac{\delta(\tau)_{nz}^{max}}{\delta\theta} (K_1, K_2, r_m, \theta_m, \tau_{ij}) \right\} = 0 \quad (4)$$

which leads to:

$$\left(\frac{K_2}{K_1}\right)^2 - \frac{4}{3} \left(\frac{K_2}{K_1}\right) \cot 2\theta_m^\circ - \frac{1}{3} = 0 \quad (5)$$

By measuring θ_m° which is approximately in the direction of the applied load, K_2/K_1 can be determined.

Then writing the stress optic law as:

$$\tau_{nz}^{max} = \frac{fn}{2t} = \frac{K_{AP}^*}{(8\pi r)^{\frac{1}{2}}}$$

where K_{ap}^* is the mixed mode SIF, one may plot $\frac{K_{AP}^*}{\bar{\sigma}(\pi a)^{\frac{1}{2}}}$ vs. $\sqrt{r/a}$ as before, locate a linear zone and extrapolate to $r = 0$ to obtain K^* . Knowing, K^* , K_2/K_1 and θ_m° , values of K_1 and K_2 may be determined since

$$K^* = [(K_1 \sin\theta_m^\circ + 2K_2 \cos\theta_m^\circ)^2 + (K_2 \sin\theta_m^\circ)^2]^{\frac{1}{2}} \quad (6)$$

Knowing K^* and θ_m° , K_1 & K_2 can be determined from Eqs. 5 and 6. Details are found in Smith and Kobayashi [2].

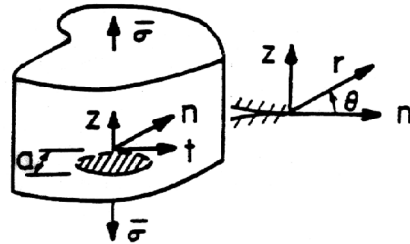


Fig. B-1 Near Tip Notation for Mode I.

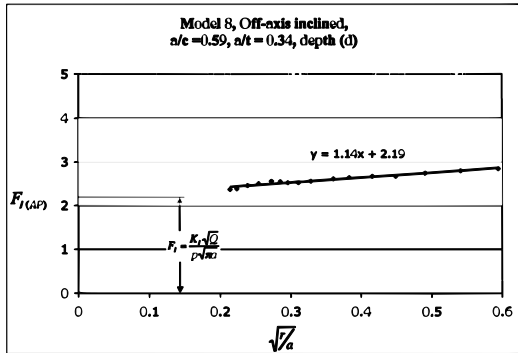


Fig. B-2: Determination of F_1 for Test Data.

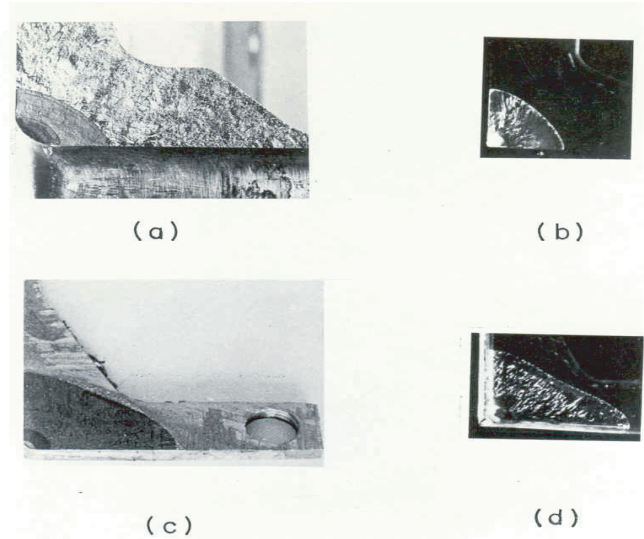


Fig. 1 Comparison of Crack Shapes from Delft Fatigued Steel Model with those grown monotonically in photoelastic model.

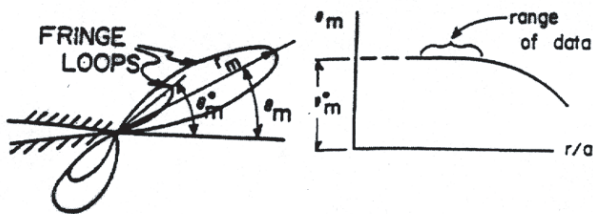


Fig. B-3: Determination of θ_m° for Mixed Mode



Fig. 2 Photoelastic Model of Nuclear Pressure Vessel Containing Two Diametrically Opposite Nozzles.

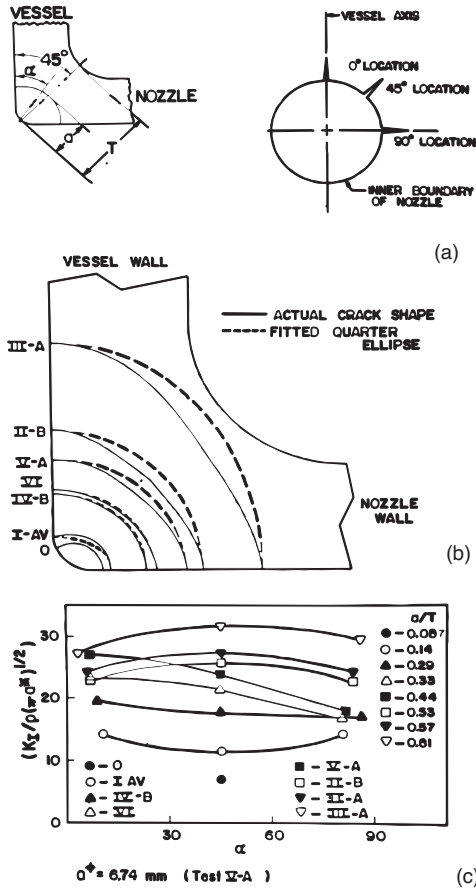


Fig. 3 a) Starter Crack Locations in Nozzle for Thin Walled Pressure Vessel b) Flattening of Crack Shapes with Increasing Depth for $\theta = 0^\circ$ c) Corresponding SIF Distributions p is internal pressure).

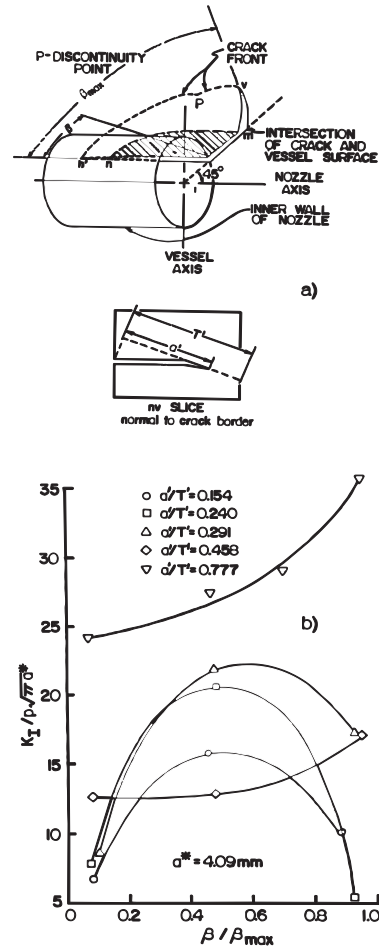


Fig. 4 a) Artist's sketch of planar crack initiated at $\theta = 45^\circ$ b) SIF Distributions for increasing crack depths.

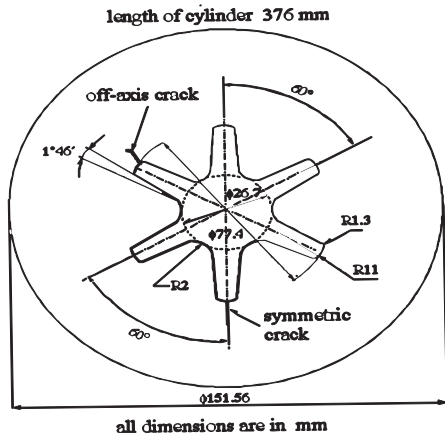
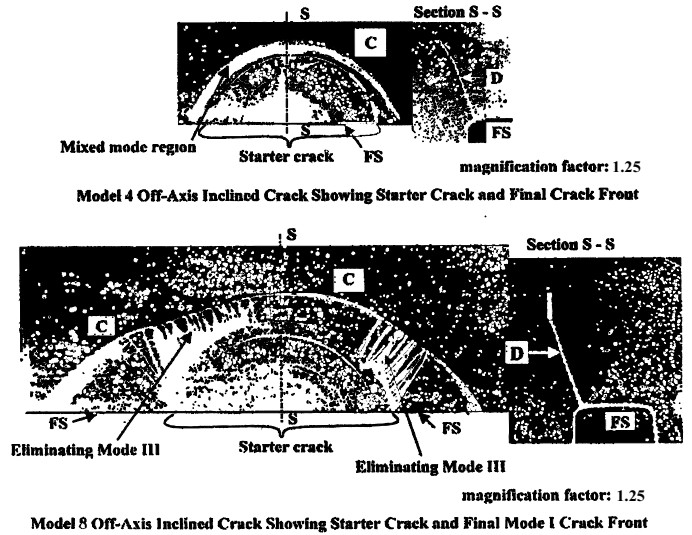


Fig. 5 Cross-section of scaled photoelastic model of motor grain showing critical crack locations.



FS – fin surface
 C – crack front
 D – camera view of the photograph

Fig. 6 Plan view of off-axis crack profiles and path of crack at its center (SS).

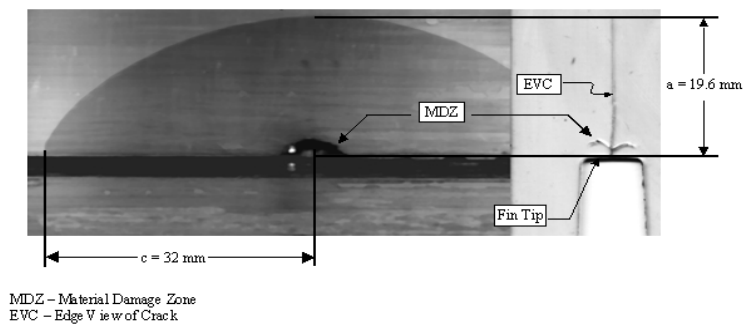


Fig. 7 Plan and cross-sectional view of a symmetric crack.